© 2016. Published by The Company of Biologists Ltd | Journal of Cell Science (2016) 129, 1416-1428 doi:10.1242/jcs.183426

RESEARCH ARTICLE

Temporal control of bidirectional lipid-droplet motion in *Drosophila* depends on the ratio of kinesin-1 and its co-factor Halo

Gurpreet K. Arora[1], Susan L. Tran[1,2,*], Nicholas Rizzo[1,‡], Ankit Jain[2,§] and Michael A. Welte[1,2,¶]

ABSTRACT

During bidirectional transport, individual cargoes move continuously back and forth along microtubule tracks, yet the cargo population overall displays directed net transport. How such transport is controlled temporally is not well understood. We analyzed this issue for bidirectionally moving lipid droplets in *Drosophila* embryos, a system in which net transport direction is developmentally controlled. By quantifying how the droplet distribution changes as embryos develop, we characterize temporal transitions in net droplet transport and identify the crucial contribution of the previously identified, but poorly characterized, transacting regulator Halo. In particular, we find that Halo is transiently expressed; rising and falling Halo levels control the switches in global distribution. Rising Halo levels have to pass a threshold before net plus-end transport is initiated. This threshold level depends on the amount of the motor kinesin-1: the more kinesin-1 is present, the more Halo is needed before net plus-end transport commences. Because Halo and kinesin-1 are present in common protein complexes, we propose that Halo acts as a rate-limiting co-factor of kinesin-1.

KEY WORDS: Bidirectional transport, Kinesin-1, Lipid droplets, *Drosophila* embryos

INTRODUCTION

Active transport along microtubules is of broad importance. It includes motion of diverse cargoes in axons and flagella, mRNA delivery for localized protein production and pigment-granule redistribution to camouflage animals. Disruptions of intracellular transport are linked to severe organismal dysfunction, including neurodegenerative and developmental disorders (Hirokawa and Noda, 2008). Microtubules are polarized filaments, and motors typically move unidirectionally along them (Vale, 2003). Although individual motor properties are increasingly well understood (Kull et al., 1996; Reck-Peterson et al., 2006; Block, 2007; Carter et al., 2011; Kon et al., 2012; Yildiz et al., 2008), many questions remain about how motors are regulated *in vivo* so that cargoes reach their destination with high spatial and temporal precision.

For some aspects of transport regulation, the underlying molecular mechanisms are well understood. For example, motor docking to cargoes can be modulated – e.g. by post-translational modifications of motors (Lee and Hollenbeck, 1995; Morfini et al., 2004) – to turn transport on or off. However, understanding cargo recognition is of limited value for determining the regulation of bidirectionally moving cargoes. Such cargoes simultaneously carry opposite-polarity motors and frequently switch direction of motion. Examples include melanosomes, secretory vesicles, mitochondria, mRNA particles, endosomes and virus particles (Welte, 2004). Imbalance in average travel distances in the two directions leads, over time, to net displacement of the cargo population. Bidirectional motion is modulated in space and time – for example, melanosomes move in response to hormonal stimuli (Aspengren et al., 2009), mitochondrial movement depends on cellular energy requirements (Sheng, 2014) and mRNA transport is controlled developmentally (Bullock et al., 2006). The key target of spatio-temporal regulation is the run length – i.e. how far a cargo travels before reversing direction. Although *in vitro* run length depends greatly on the number of motors active per cargo, to what extent docking and release of motors contributes to run-length control *in vivo* is unclear. In at least some cases, run length is independent of the number of active motors (Shubeita et al., 2008), suggesting that some tuneable 'switching' mechanism ends runs (Gross et al., 2000).

Exquisite temporal regulation of run length is characteristic of bidirectional lipid-droplet motion in early *Drosophila* embryos (Welte, 2015). Here, microtubules are radially arranged, with plus ends towards the embryo centre and minus ends towards the periphery. Lipid-droplet motion is powered by the plus-end-directed kinesin-1 (Shubeita et al., 2008) and the minus-end-directed cytoplasmic dynein (Gross et al., 2000). Motor activity is temporally regulated, resulting in global shifts of the droplet population during embryogenesis. Initially (phase I, nuclear cycles 11–12), run lengths for the two directions are balanced; although individual droplets move constantly, the droplet population remains broadly distributed throughout the periphery. In phase IIa (cycle 13 to mid-cellularization), upregulation of plus-end run lengths causes a plus-end (inward) shift of the droplet population. During phase IIb (a 10-min period near the end of cellularization), travel lengths for both directions become similar, and the droplet population shifts towards the minus ends. This outward shift continues through gastrulation (phase III) when specifically plus-end runs shorten. Genetic and biochemical approaches have identified four components of the transport machinery that are important for proper control of run length – LSD-2 (Welte et al., 2005), Klar (Welte et al., 1998; Guo et al., 2005), Dynactin (Gross et al., 2002) and BicD (Larsen et al., 2008). All four regulators are maternally provided to the embryos and present in all phases; therefore, they alone cannot explain how transport is temporally regulated.

A key mediator of temporal control is the Halo protein, a droplet-specific factor whose mRNA is newly expressed just as phase IIa starts. Halo is necessary for the phase-I to phase-IIa transition, upregulating plus-end and downregulating minus-end run lengths (Gross et al., 2003). Several lines of evidence exclude that Halo acts by recruiting motors – the amount of kinesin on droplets is

[1]Department of Biology, University of Rochester, Rochester, NY, USA. [2]Department of Biology, Brandeis University, Waltham, MA, USA.
*Present address: Boston Biomedical INC, Sumitomo Dianippon Pharma Global Oncology, Cambridge, MA, USA. ‡Present address: Department of Biology, Duke University, Durham, NC, USA. §Present address: Department of Neuroscience, Perelman School of Medicine at the University of Pennsylvania, Philadelphia, PA, USA.

¶Author for correspondence (michael.welte@rochester.edu)

Received 29 November 2015; Accepted 15 February 2016

Journal of Cell Science

Journal of Cell Science (2016) 129, 1416-1428 doi:10.1242/jcs.183426

unchanged from phase I to phase IIa, and – in any case – droplet run length is independent of motor copy number (Shubeita et al., 2008). Previous work suggests that Halo acts as a transcription factor (Bonneaud et al., 2003) or by controlling LSD-2 modification (Welte et al., 2005).

We find that Halo is the crucial timer that controls transitions between phases. Halo protein is transiently expressed during phase II; onset and degradation of Halo promote the switch from phase I to phase IIa and from phase IIa to phase IIb and/or phase III, respectively. We find that Halo initiates a net plus-end shift of the droplet population only once it reaches a certain threshold. We rule out that Halo controls droplet motion by regulating transcription or by acting solely through LSD-2. Instead, we discover that kinesin-1 levels set the threshold for Halo action, possibly through a physical interaction. We propose that transiently expressed Halo acts as a limiting co-factor of kinesin-1.

RESULTS

Halo promotes net plus-end transport in phase II

We captured the temporal pattern of droplet distribution (Fig. 1A,B) by staining for the droplet protein Jabba (Li et al., 2012). Inhibiting zygotic transcription prevents the switch to net plus-end droplet motion in phase IIa (Merrill et al., 1988). This defect is due to the absence of a single genetic locus because embryos homozygous for the deletion Δ(*halo*) display the same phenotype (Gross et al., 2003). *halo* was identified as the crucial gene in this deletion because injection of *halo* double-stranded (ds)RNA (i.e. to inhibit *halo* expression through RNA interference) into wild-type embryos causes a similar defect, and *in vitro* generated *halo* mRNA restores inward transport in Δ(*halo*) embryos (Gross et al., 2003).

We developed additional reagents to modulate Halo expression, including the smaller deletion $\Delta halo^{AJ}$ (Rembold et al., 2014) and the point allele $halo^{GA}$. Embryos homozygous for $\Delta halo^{AJ}$ (Fig. 1C) or

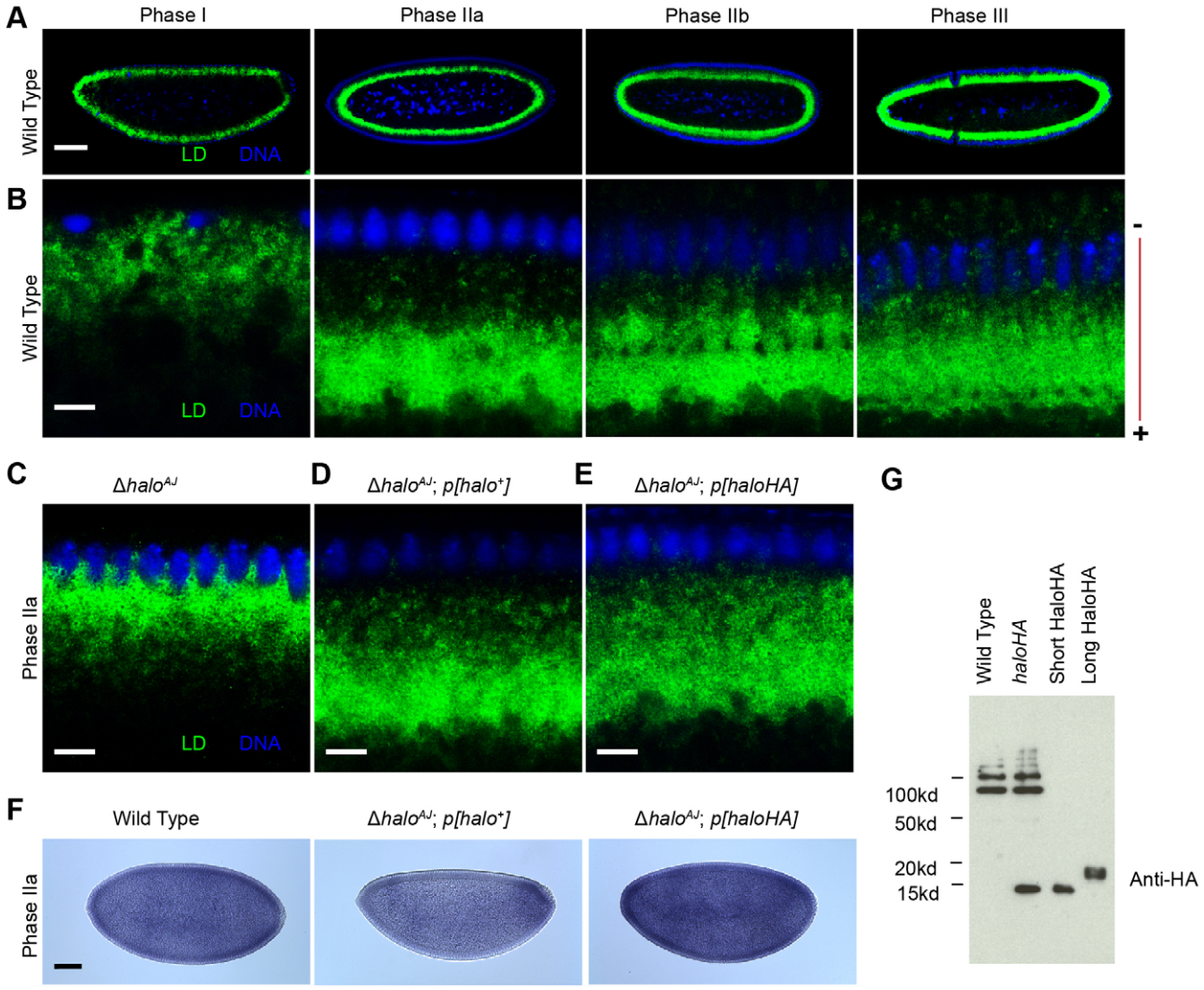

Fig. 1. *Halo* locus promotes net plus-end transport in phase II. (A–E) Lipid-droplet (LD) distribution in embryos, revealed by staining for Jabba (green) and nuclei (blue). (A,B) In wild-type embryos, droplets are broadly distributed in the peripheral cytoplasm in phase I, and move inward in phase IIa. This is followed by outward redistribution during phase IIb and phase III. Panels depict either the entire embryo (A) or a section of the periphery (B); the bar on the right in B indicates the approximate location, orientation and polarity of microtubules in these micrographs. (C) Lipid droplets are mislocalized during phase IIa in $\Delta halo^{AJ}$ embryos (also referred to as *halo* or 0× $halo^{+}$ in the rest of the paper). (D,E) Inward droplet accumulation during phase IIa is restored if *halo* embryos express genomic $halo^{+}$ transgenes. (F) *In situ* hybridization for *halo* mRNA. (G) Anti-HA immunoblotting of wild-type and *p[haloHA]* embryos, and of pellets from bacteria expressing two different sizes of Halo–HA, based on the two annotated start sites. The high-molecular-mass bands present in both wild-type and *p[haloHA]* embryos are due to non-specific cross-reactivity and serve as loading controls. Scale bars: 7.5 µm (B–E); 75 µm (A,F). Representative examples of at least three independently performed experiments are shown.

Journal of Cell Science (2016) 129, 1416-1428 doi:10.1242/jcs.183426

halo^{GA} (not shown) lacked inward droplet transport during phase IIa, indistinguishable from that in Δ(*halo*) embryos (Gross et al., 2003). We generated a genomic *halo* construct (*p[halo]*); in the Δ*halo*^{AJ} background, this transgene was expressed in a pattern similar to that of wild-type *halo*, although at reduced levels (Fig. 1F). Two transgene copies restored net inward droplet transport substantially, although not completely (Fig. 1D). This less extensive inward transport is likely to be due to insufficient Halo expression (Fig. 1F) because it is also observed in embryos heterozygous for Δ(*halo*) (Gross et al., 2003). Taken together, our findings corroborate that *halo* is responsible for net-inward transport of droplets in phase II.

Halo mRNA contains two predicted in-frame translation start sites, corresponding to Halo proteins of 109 or 150 amino acids (Gross et al., 2003). To determine which variant is expressed, we introduced a *halo* genomic transgene with three copies of the hemagglutinin (HA) tag (*p[haloHA]*) into the Δ*halo*^{AJ} background. *Halo* message was expressed at levels similar to those of the wild type (Fig. 1F); the temporal pattern was also similar (not shown). Two copies of *p[haloHA]* in a Δ*halo*^{AJ} background promoted substantial net-inward displacement of lipid droplets (Fig. 1E, compare to Fig. 1C). Thus, the tagged protein was functional, although potentially less efficient or less stable. By western blotting analysis of *p[haloHA]* embryos, we detected one major Halo–HA form that, when compared to bacterially expressed versions of Halo–HA, co-migrated with the 109-amino-acid form (Fig. 1G). We conclude that, *in vivo*, the second translation start site is used, which also corresponds to the single predicted translation start of most Halo orthologues in other *Drosophila* species (see, for example, Gross et al., 2003).

Rising and falling Halo levels drive transitions between phases

Halo mRNA is first detected at the phase-I to phase-IIa transition and declines rapidly at the end of phase IIa (Gross et al., 2003). Immunostaining (Fig. 2Aa–Ae) and western blotting (Fig. 2B) revealed that the expression of Halo protein closely mimics this pattern – the protein was first detectable in late phase I, its levels peaked in phase IIa, declined in phase IIb and were drastically lower in phase III (Fig. 2Aa–Ae). As Halo is required for the phase-I to phase-IIa transition (Gross et al., 2003), the rapid rise in

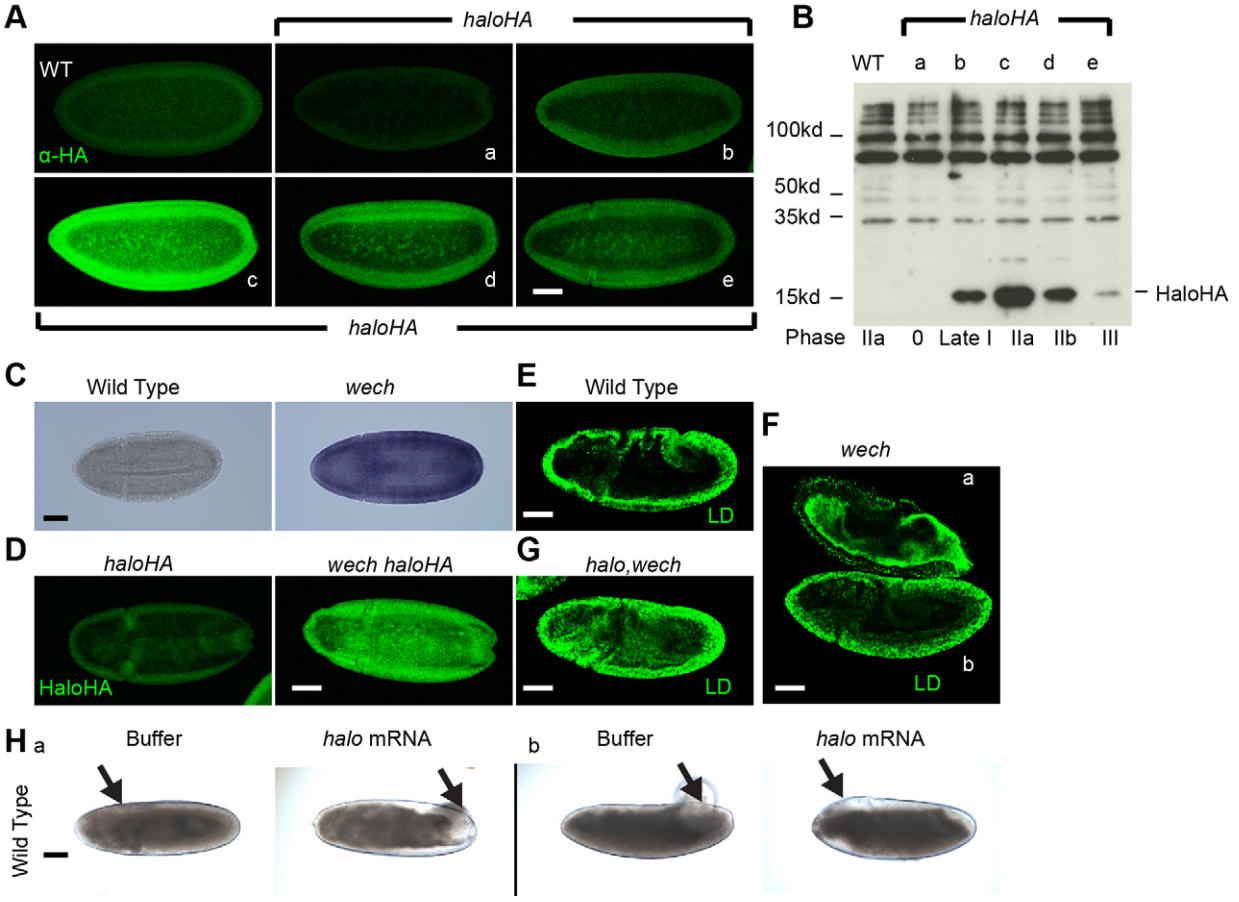

Fig. 2. The onset and degradation of Halo promote transitions between phases. (A) Detection of HA (α-HA) in wild-type (phase IIa, WT) and *p[haloHA]* embryos. Halo is absent in cleavage-stage embryos (a) and is first detected during late phase I (cycle 13, b), with levels rising into phase IIa (c) and declining in phase IIb (d), and levels are drastically reduced in phase III (e). (B) Immunoblotting for HA by using equal numbers of fixed embryos (same ages as in A) reveals the same transient (less than 1.5 h) pattern. (C) *In situ* hybridization for *halo* mRNA. In phase III, *halo* message is barely detectable in wild-type embryos, but remains high in *wech* embryos. (D) Immunostaining for HA in phase-III embryos reveals increased Halo levels in *wech* versus wild-type embryos. (E–G) Staining for Jabba to assess droplet (LD) distribution in phase-III embryos. (E) Lipid droplets are present throughout the embryo periphery in the wild type. (Fa) In embryos lacking both the maternal and zygotic supply of *wech*, droplets remain inward, as in phase IIa. (Fb) In embryos lacking only the maternal supply of *wech*, the droplet distribution resembles that of wild type. (G) In embryos lacking both *wech* and *halo*, droplets are peripheral. (H) Wild-type embryos in early phase III that had been injected during late phase IIa. Arrows indicate injection site. (a,b) Embryos that had been injected with *halo* mRNA remain transparent around the injection site. Buffer-injected embryos have an opaque periphery everywhere. Scale bars: 75 µm. Representative examples of at least three independently performed experiments are shown.

Journal of Cell Science (2016) 129, 1416-1428 doi:10.1242/jcs.183426

Halo levels is functionally important. Because Halo levels drop just when transport reverses (Fig. 1A), these events might be mechanistically related. We thus sought to extend Halo expression into phase III.

Interference with the TRIM-NHL family member Wech, by injecting dsRNAs into embryos to inhibit *Wech* expression, results in droplet mislocalization in phase III (Pilot et al., 2006). Because Wech's mammalian orthologue TRIM71 promotes accelerated mRNA decay (Loedige et al., 2013), Wech might affect transport through regulation of gene expression. We identified a missense mutation (*wech*^{7}) in a highly conserved amino acid residue of Wech. Embryos homo- or hemizygous for *wech*^{7} are viable, and mothers hemizygous for *wech*^{7} are fertile, but *wech*^{7} homozygous embryos laid by such mothers die. These results suggest that Wech function can be supplied both maternally and zygotically, consistent with the previously described maternal and zygotic expression pattern of *wech* mRNA (Pilot et al., 2006).

In embryos in which both supplies of Wech had been compromised, *halo* message persisted through phase III (Fig. 2C). Halo protein expression displayed the same temporal pattern, persisting into phase III (Fig. 2D). Thus, Wech is necessary for the decline of Halo protein levels in phase IIb and phase III. This extension of Halo expression was associated with dramatically altered droplet transport (Fig. 2F). In embryos that lacked normal Wech function both maternally and zygotically, droplet transport failed to reverse in phase III, and droplets remained inwardly distributed (Fig. 2Fa). In contrast, in embryos in which Wech function was provided either maternally or zygotically (Fig. 2Fb), droplets shifted outward, just like in wild-type embryos (Fig. 2E).

This abnormal droplet transport might be due to Halo-independent roles of Wech or the continued presence of Halo. We favour the second possibility because the *wech* mutant phenotype depends on Halo – in embryos that lacked both Halo and Wech function, lipid droplets were peripheral in phase III (Fig. 2G), consistent with the idea that persistent Halo prevents the switch to outward transport. This notion is further supported by ectopic Halo expression. Because lipid droplets scatter light, cytoplasm that is full of droplets is opaque (Welte et al., 1998). In wild-type embryos, and in buffer-injected embryos (Fig. 2Hb), the periphery thus turns from transparent to opaque in phase III. Yet, in wild-type embryos that had been injected with *halo* mRNA during late phase IIa, the region near the injection site remained transparent in phase III, indicating that extra Halo locally suppresses outward droplet transport (Fig. 2Ha).

In summary, Halo is the key factor controlling two transitions in droplet transport – Halo synthesis promotes the phase-I to phase-IIa transition, and loss of Halo is necessary for the phase IIa to phase-IIb–phase-III transition.

Quantifying the effect of Halo during phase transitions

We next determined the time course of droplet distribution during these Halo-driven transitions. We classified embryos into eight age classes (t0 to t7) based on morphological changes that occur as embryos develop from a syncytium to a cellularized blastoderm – change in number of nuclei (to determine mitotic cycles), shape of nuclei and extent of plasma membrane invagination (Foe and Alberts, 1983). At 25°C, these age classes represent a total time period of ∼70 min (Surkova et al., 2008). During cycle 12, when Halo is undetectable, the droplet distribution of wild-type and *halo* embryos was indistinguishable (Fig. 3A t0, 3D t0 and E; Table S1). During cycle 13, when Halo is first detected, the droplet population in wild-type embryos shifted inward (Fig. 3At1) and continued to shift further inwards during early cycle 14 (Fig. 3A t2 to t6). Once the membranes had grown beyond the nuclei (corresponding to the phase-IIa to phase-IIb transition), the droplet population started to shift outwards (Fig. 3A t7).

To quantify the droplet distribution, we measured the intensity of Jabba signal along six apically–basally oriented lines per embryo and averaged the normalized intensities. Using this approach, we could estimate, for each position along the apical–basal axis, the fraction of the population present at this position (Fig. 3B) or between this position and the apical tip of the nuclei (Fig. 3C). These data reveal, for example, the dramatic inward shift of the overall droplet distribution between cycle 13 (phase-I to phase-IIa transition) (Fig. 3A t1) and late phase IIa (Fig. 3A t6). In most age classes, the normalized distributions were very similar between embryos, and the average position of the droplet population was well defined (see error bars in Fig. 3E). Using this approach, we uncovered statistically significant shifts in mean distribution, even between stages that by eye appeared to be indistinguishable (e.g. t3 versus t5, Fig. 3E legend). The maximal inward shift in average droplet position was ∼8 µm (Fig. 3E), consistent with previous estimates using electron microscopy (Welte et al., 1998).

To determine Halo's contribution, we performed a similar time-course analysis for Δ*halo*^{4J} embryos (Fig. 3D). Here, the droplet population gradually shifts outward as development proceeds (Fig. 3D,E). Thus, in addition to Halo, other inputs modulate droplet transport, although their molecular nature remains unknown (Gross et al., 2003). The difference in average droplet position between wild-type and *halo* mutants represents the contribution of Halo to transport kinetics (Fig. 3F).

A threshold for Halo action

We next determined the time course of Halo expression for these transitions (Fig. 3G). Levels rose steadily from t1 onwards, peaked around t4 and then dropped. Halo's rise and fall foreshadows the inward and outward shift of the droplet population. We therefore asked whether the exact levels of Halo are important for phase transitions.

We manipulated Halo levels experimentally by changing *halo*$^{+}$ gene dosage. By western analysis, Halo–HA levels in embryos with two copies of the transgene were roughly double those of embryos with one transgene, regardless of the genotype at the endogenous *halo*$^{+}$ locus (Fig. 4E). Using Δ*halo*^{4J} and a duplication of the *halo*$^{+}$ genomic region, we generated embryos carrying zero (0×), one (1×), two (2×) or four (4×) copies of *halo*$^{+}$. *In situ* hybridization revealed that the intensity of the *halo* signal during phase II corresponded to *halo*$^{+}$ copy number (Fig. 4D), although the pattern of the rise and decline of *halo* mRNA was unaffected (not shown).

These dosage changes dramatically altered droplet transport kinetics (Fig. 4A–C). At t0, all four genotypes exhibited similar droplet distributions. From t1 onwards, increased *halo* dosage resulted in both an earlier inward shift and, at a given age, overall greater inward displacement. The difference between genotypes was particularly obvious at early stages – for example, at t1, 4× *halo*$^{+}$ embryos displayed a significant inward shift compared to 2× *halo*$^{+}$ embryos; however, 0× *halo*$^{+}$ and 1× *halo*$^{+}$ embryos were indistinguishable (Fig. 4C; Table S1). We hypothesize that the net inward shift is only initiated once Halo levels pass a threshold; with increasing *halo*$^{+}$ copy number, this threshold is reached earlier, leading to increasingly earlier net-inward shifts.

If this threshold model is correct, lowering *halo*$^{+}$ levels even more should delay transport further. The tagged transgene *p[haloHA]* is partially compromised in expression or function (Fig. 1E). At t1, embryos expressing one or two copies of the transgene in a *halo*

Journal of Cell Science (2016) 129, 1416-1428 doi:10.1242/jcs.183426

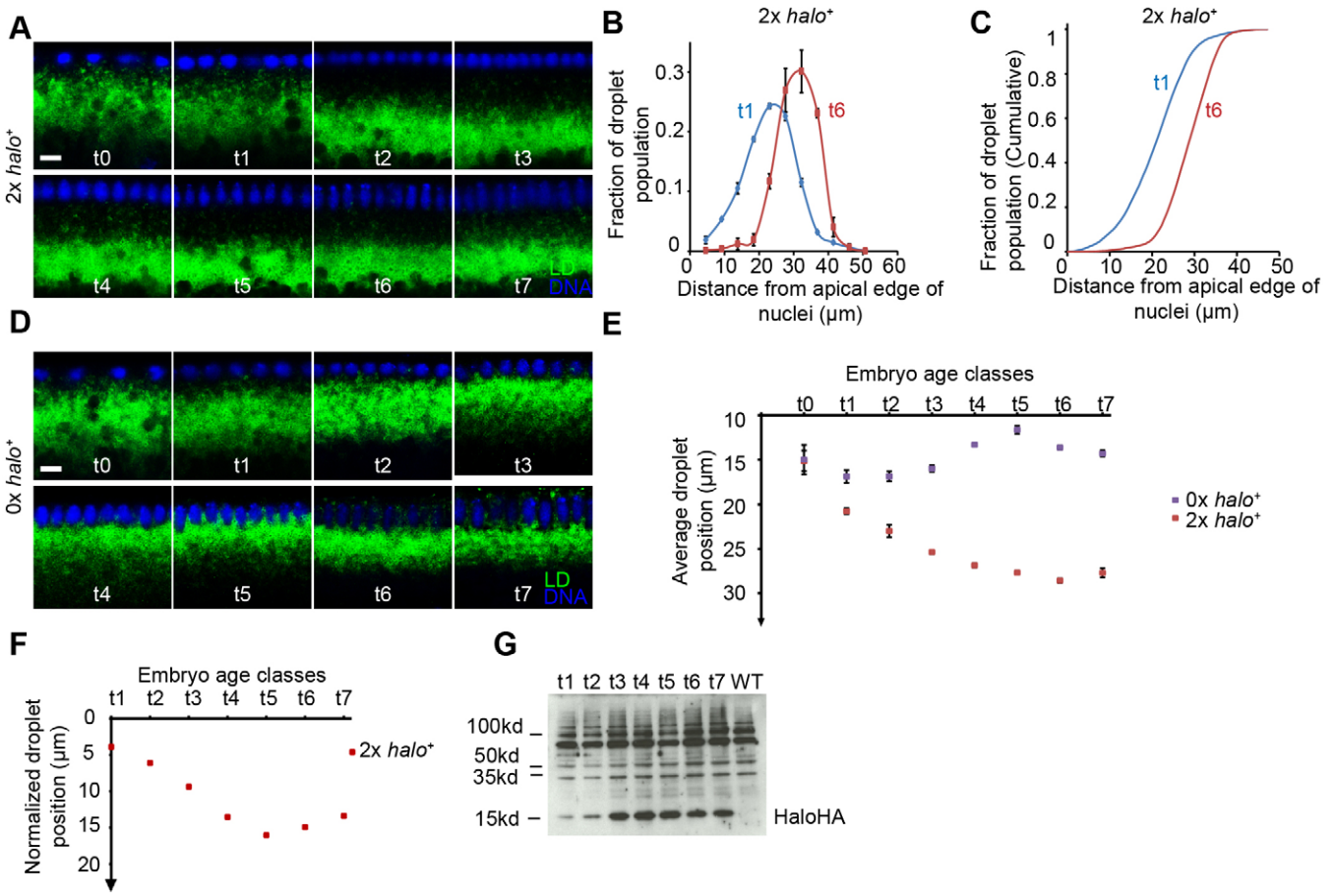

Fig. 3. Halo levels are crucial for the temporal regulation of droplet transport. (A,D) Staining of Jabba (green) in embryos classified into eight temporal classes (t0 to t7) – cycle 12 (t0, phase I), cycle 13 (t1, phase-I to phase-IIa transition), cycle 14 (t2–t6, phase IIa), late cycle 14 (t7, phase-IIa to phase-IIb transition). Nuclei are blue. (A) In wild-type (WT) embryos, the droplet population continuously shifts inwards from t1 onwards, followed by a reversal at t7. (B,C) Droplet distribution in wild-type embryos at t1 and t6. The fraction of the droplet population (B) and the cumulative population of the droplets (C) along the apical–basal axis of embryos as a function of distance from the apical edge of the nuclei. (D) In *halo* embryos, the droplet population moves outwards over time. (E) Average droplet position as a function of time for wild-type and *halo* embryos. The apparent inward shift for *halo* embryos during t6 and t7 is likely to result from droplets being excluded by increasingly larger nuclei. (B,E) Data are presented as mean±s.d. of three embryos. At each age class, apart from t0, there is a significant difference in the average droplet position between wild-type and *halo* embryos (Table S1). In the wild type, average droplet position is significantly different between t3 and t5 ($P \leq 0.001$, see Table S1), as assessed by *t*-test. Plots in B,C,E are based on the same dataset. (F) Difference in the average position of the droplets between wild-type and *halo* embryos for each age class. (G) Immunoblotting for HA by using equal numbers of *haloHA* embryos from t1 to t7. Wild-type embryos serve as negative control. Scale bars: 7.5 μm (A,D). Representative examples of at least three independently performed experiments are shown with the exception of the experiment shown in G, which was done twice.

background (1× *haloHA* and 2× *haloHA*, respectively) were indistinguishable from *halo* embryos (Fig. 4F,G; Table S2). At time t4, when 2× *haloHA* embryos displayed an inward shift of droplets, the average droplet position of 1× *haloHA* and *halo* mutant embryos remained statistically indistinguishable (Fig. 4G; Table S2). We conclude that as Halo levels rise developmentally, they have to pass a threshold before Halo affects droplet distribution.

Halo protein is broadly distributed

To understand this threshold effect, we next sought to determine how Halo acts at the molecular level. Halo is necessary for longer plus-end runs in phase IIa (Gross et al., 2003) and, thus, ultimately controls properties of kinesin-1. Two previous studies have suggested that Halo affects kinesin-1 indirectly – Halo might act by regulating transcription (Bonneaud et al., 2003) or by altering lipid-droplet proteins (Welte et al., 2005).

These models make distinct predictions about the cellular location of Halo. Immunostaining revealed that Halo is present both in the nucleus and broadly throughout the cytoplasm (Fig. 5A). We used *in vivo* centrifugation to separate lipid droplets from other embryonic components (Cermelli et al., 2006; Tran and Welte, 2010); staining for HA revealed that a fraction of the Halo signal was associated with the droplet layer (Fig. 5B). By western blotting analysis, Halo was also enriched in biochemically purified lipid-droplet preparations, compared to those prepared from embryo lysate, although not as massively as the established droplet protein LSD-2 (Fig. 5C). Thus, both imaging and biochemical analyses suggest that Halo is present on lipid droplets.

In summary, Halo is present in the nucleus, on lipid droplets and elsewhere in the cytoplasm. Because this distribution does not allow us to distinguish between the proposed models of Halo action, we next examined crucial features of each model individually.

Halo regulates transport neither by regulating transcription nor by solely acting through LSD-2

The Halo paralogue SNCF has been reported to be a co-factor for the transcriptional regulator Sox Neuro (Bonneaud et al., 2003). To test

Journal of Cell Science (2016) 129, 1416-1428 doi:10.1242/jcs.183426

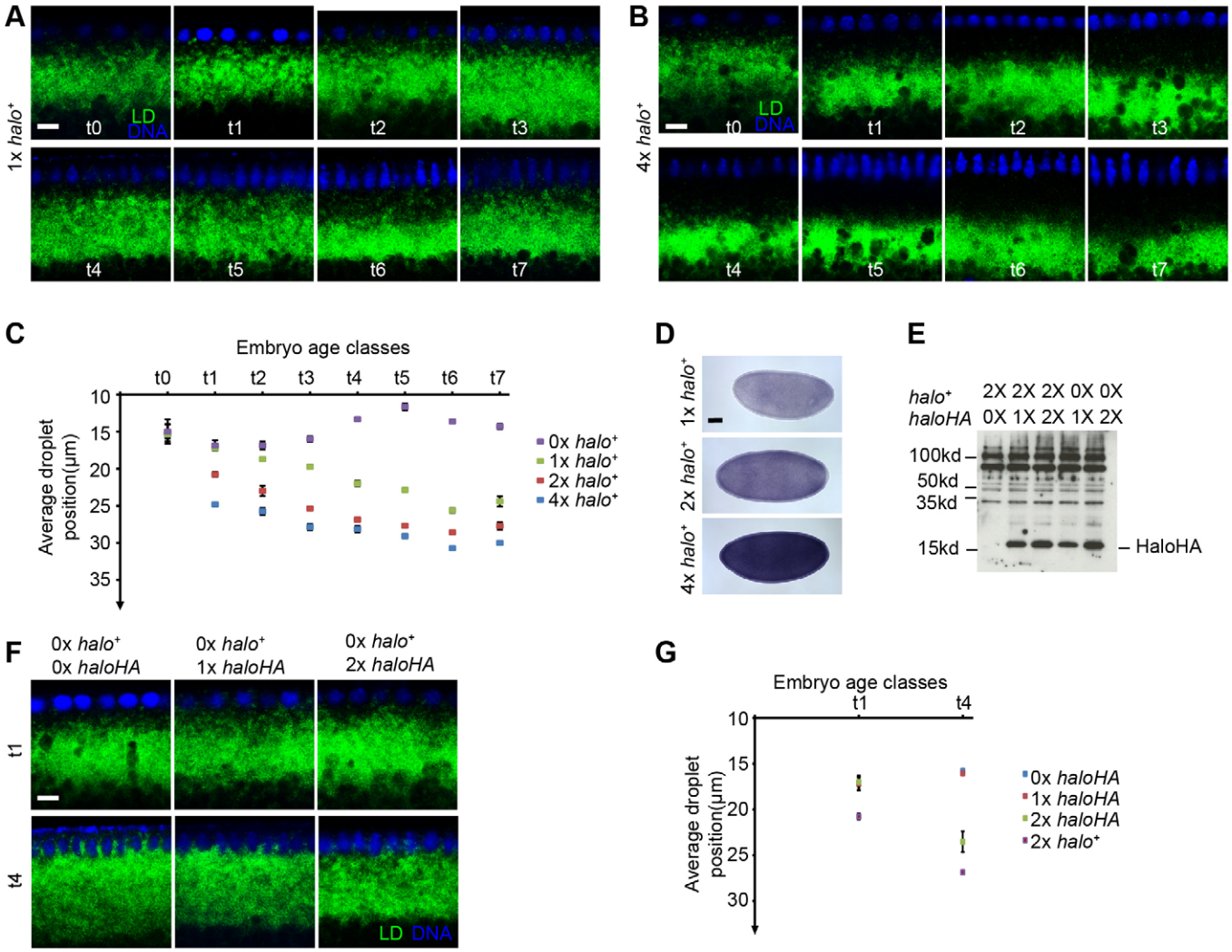

Fig. 4. Halo levels need to surpass a threshold to affect droplet transport. (A,B) Droplet (LD) distribution in embryos expressing 1× *halo*$^{+}$ and 4× *halo*$^{+}$, as revealed by staining for Jabba (green). Nuclei are blue. (C) Average droplet position over time in embryos of different *halo*$^{+}$ dosages. The data for 0× and 2× *halo*$^{+}$ embryos are the same as in Fig. 3E. There is no statistical significant difference between all genotypes at t0 (Table S1). At t1, the droplets move inwards earlier in embryos expressing 4× *halo*$^{+}$, whereas in embryos expressing 1× *halo*$^{+}$, the droplet position is indistinguishable from 0× *halo*$^{+}$ embryos (Table S1). (D) *In situ* hybridization for *halo* message in embryos expressing 1×, 2× or 4× *halo*$^{+}$. (E) Immunoblot for HA by using phase-IIa embryos expressing 1× or 2× *haloHA* in a wild-type or *halo* background. Halo protein levels change with gene dosage. (F) Staining for Jabba in t1 and t4 embryos expressing 0×, 1× or 2× *haloHA* in a *halo* background. (G) At t1, the average droplet position is indistinguishable for 0×, 1× or 2× *haloHA* embryos. At t4, 0× and 1× *haloHA* embryos remain indistinguishable, whereas 2× *haloHA* embryos have diverged, displaying an inward shift (see Table S2 for *P*-values). (C,G) Data are presented as mean±s.d. of three embryos. Scale bars: 7.5 µm (A,B,F); 75 µm (D). Representative examples of at least three independently performed experiments are shown.

whether Halo affects transport by regulating transcription, we asked whether Halo can still promote net plus-end transport when transcription is inhibited pharmacologically. We first injected wild-type phase-I embryos with the RNA polymerase inhibitor α-amanitin. Such embryos develop until phase IIa but do not transcribe *halo* and fail to undergo net-inward transport of lipid droplets. As a result, the peripheral cytoplasm remains opaque in phase IIa (Gross et al., 2003). Once the embryos had developed this opaque periphery, we injected them with *in-vitro*-generated *halo* mRNA. Near the injection site, the cytoplasm became transparent, indicating net inward droplet transport (Fig. 5D). We conclude that Halo can promote plus-end transport, even in the absence of transcription.

LSD-2, a member of the Perilipin family of lipid-droplet-associated proteins, is, directly or indirectly, a target of Halo (Welte et al., 2005). LSD-2 is phosphorylated at multiple residues and undergoes phase-specific changes in its phosphorylation state that depend on Halo (Welte et al., 2005). Because LSD-2 regulates droplet transport (Welte et al., 2005), the phase-IIa inward shift of lipid droplets is reduced in embryos that lack *LSD-2* (Fig. 5E). *LSD-2 halo* double-mutant embryos displayed droplet accumulation below the nuclei; thus, the droplets are shifted outward, compared to their position in *LSD-2* single mutants (Fig. 5E). Thus, Halo can affect droplet transport in the absence of LSD-2, and Halo must have other targets.

The kinesin-1:Halo ratio is crucial for correct transport

Might the crucial target of Halo be the plus-end motor itself? Halo and kinesin-1 exhibit a similar broad cytoplasmic distribution (Fig. 6A), with a fraction of each being associated with lipid droplets (Fig. 6B). They both promote plus-end transport because absence of either leads to failure of inward transport during phase IIa (Gross et al., 2003; Shubeita et al., 2008). If they act synergistically,

Journal of Cell Science (2016) 129, 1416-1428 doi:10.1242/jcs.183426

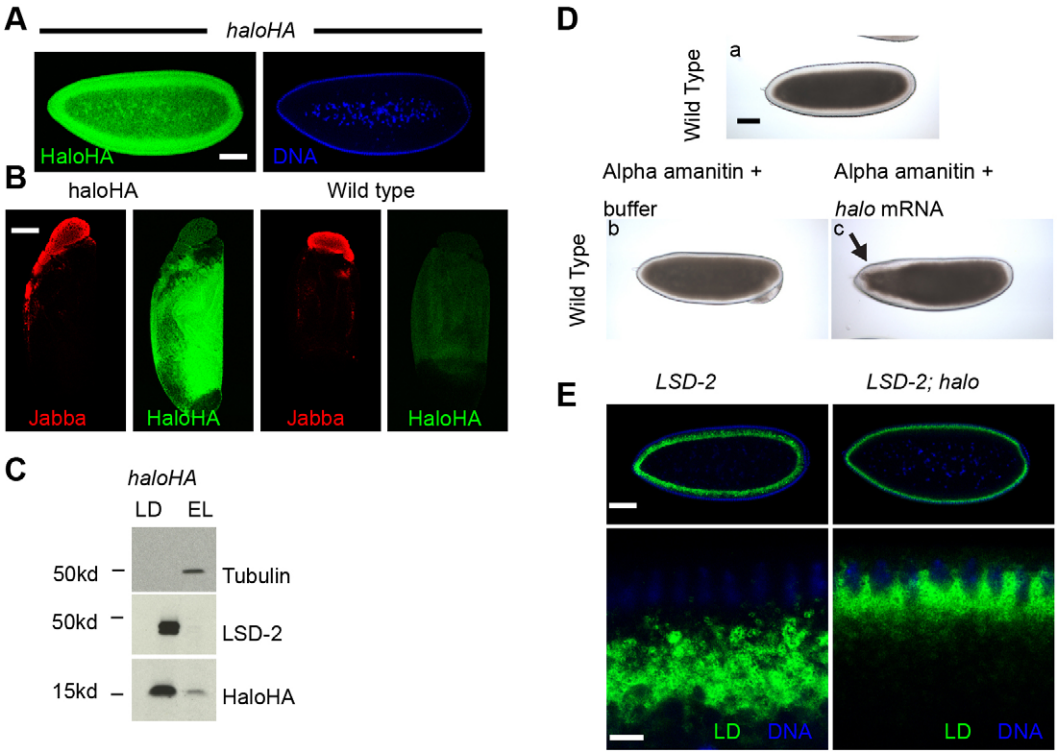

Fig. 5. Halo does not control transport by regulating transcription or acting solely through LSD-2. (A) Staining for HA in wild-type and *haloHA* embryos. Halo localizes to both nuclei and cytoplasm. (B) Staining for Jabba (red) and HA (green) in centrifuged, heat-fixed wild-type and *haloHA* embryos. Some Halo associates with the droplet layer (marked by Jabba). Wild-type embryos act as negative control. (C) Equal amounts of protein from *haloHA* lipid-droplet samples (LD) and whole-embryo lysate (EL) analyzed by immunoblotting. The droplet fraction is highly enriched for the droplet protein LSD-2 and depleted for the cytoplasmic protein tubulin. Because the droplet proteome is less complex than that of the lysate, the increased Halo signal in the LD lane indicates that Halo is relatively more abundant in the droplet fraction than in the embryo as a whole. As the enrichment is much less than that for LSD-2 (at these exposures, LSD-2 signal in the lysate is undetectable), Halo must also be present elsewhere. (D) Injection of wild-type (a) embryos with α-amanitin followed by re-injection with *halo* mRNA (c) or buffer alone (b). α-Amanitin causes droplets to move outwards (b), similar to the situation in *halo* embryos (opaque periphery), and on re-injection with *halo* mRNA, the droplets move inward near the injection site (transparent region), similar to what is seen in panel Da. Arrow indicates injection site. (E) Staining of Jabba in *LSD-2* and *LSD-2;halo* embryos. In *halo;LSD-2* double mutants, droplets are shifted outward, compared to their position in *LSD-2* embryos. Scale bars: 7.5 µm (E, bottom row); 75 µm (A,B,D,E, top row). Representative examples of at least three independently performed experiments are shown.

simultaneous mild impairment of both should cause a much more dramatic disruption in transport.

We thus reduced Halo and kinesin-1 levels in parallel. Kinesin-1 is maternally provided, and kinesin heavy chain (Khc) protein levels in the embryo scale with *Khc* dosage in the mother. In particular, mothers heterozygous for the null allele Khc^{27} produce embryos (referred to hereafter as 1× *Khc*) with approximately half as much Khc overall and reduced Khc levels on lipid droplets (Shubeita et al., 2008). We crossed such mothers to *halo*-mutant fathers to obtain embryos with reduced dosage of both molecules (1× *Khc* 1× $halo^{+}$). As shown earlier, transport was delayed in 2× *Khc* 1× $halo^{+}$ embryos (Fig. 4C, 1× $halo^{+}$). Yet, in 1× *Khc* 1× $halo^{+}$ embryos, transport kinetics closely mimicked those in the wild type (2× *Khc* 2× $halo^{+}$) at both t1 and t4 (Figs 6C and 2E; Table S3). This unexpected result can be explained if reduced Khc levels somehow promote inward transport. But, in 2× *Khc* 0× $halo^{+}$ and 1× *Khc* 0× $halo^{+}$ embryos, droplet distribution was indistinguishable over the entire time course analyzed (Fig. 6G,H). Thus, the effect of altered Khc dosage depends on Halo, suggesting a specific genetic interaction. In particular, we conclude that less Halo is required for efficient plus-end transport if kinesin-1 availability is reduced.

We also increased the amount of Khc beyond wild-type levels, by using an ubiquitin–Khc transgene (Brendza et al., 2000). By immunoblotting, Khc levels in the embryos from such mothers were approximately four times higher than those in wild type (not shown). Net plus-end transport during phase IIa was severely impaired (Fig. 6D), and additional copies of *halo* relieved the delay in transport (Fig. 6D,F; Table S4). In turn, when embryos from such mothers carried only a single copy of *halo*, net plus-end transport was compromised even further (Fig. 6D). We conclude that it is the kinesin-1:Halo ratio, not the absolute amount of either Halo or Khc, that controls droplet transport in phase II.

During the phase-I to phase-IIa transition, Halo has to surpass a threshold before net inward transport commences (Fig. 4). For example, at time t1, 2× *Khc* 0× $halo^{+}$ and 2× *Khc* 1× $halo^{+}$ embryos were still indistinguishable, whereas 2× *Khc* 2× $halo^{+}$ embryos already showed an inward shift in droplet distribution. When kinesin-1 levels were reduced, the 1× $halo^{+}$ embryos already showed this inward shift at time t1 (1× *Khc* 1× $halo^{+}$ embryos), indicating that the threshold for Halo had shifted. In embryos expressing 1× or 2× $halo^{+}$ in the *Khc*-overexpression background, the droplet distribution was indistinguishable at t1 (Fig. 6F; Table S4), unlike in the wild-type background, indicating that, at increased kinesin-1 levels, more Halo is required to surpass the threshold.

We propose that it is the amount of kinesin-1 that sets the threshold for Halo action. To test this further, we examined embryos expressing a single copy of the HA-tagged transgene (in the *halo* background); such 2× *Khc* 1× *haloHA* embryos were indistinguishable from 2× *Khc* 0× $halo^{+}$ embryos at ages t1 and t4 (Fig. 4G); at t4, the droplets had even shifted outward and accumulated below the nuclei,

Journal of Cell Science (2016) 129, 1416-1428 doi:10.1242/jcs.183426

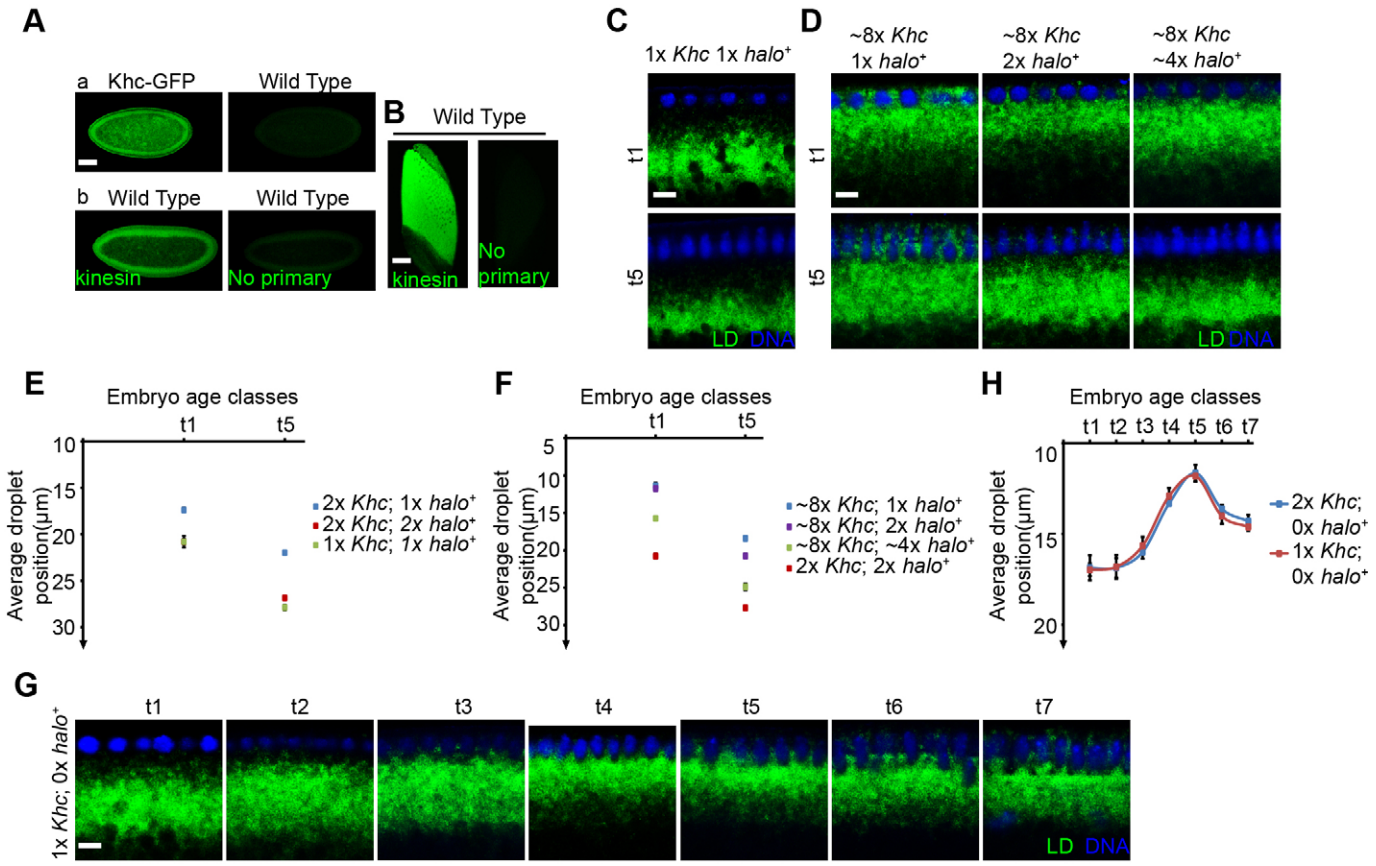

Fig. 6. The kinesin-1:Halo ratio is crucial for correct droplet transport. (Aa) The Khc–GFP signal reveals the broad cytoplasmic distribution of kinesin-1. Wild-type embryos serve as negative control. (Ab,B) Staining of kinesin-1 in uncentrifuged (Ab) and centrifuged wild-type embryos (B). Kinesin is broadly distributed in the cytoplasm (A), and a small fraction associates with the droplet layer (B). (C,D) Staining of Jabba in embryos expressing different ratios of kinesin-1 to Halo, age classes t1 and t5. (C) Global droplet distribution in 1× *Khc*; 1× *halo*$^{+}$ embryos is similar to that of wild-type (2× *Khc*; 2× *halo*$^{+}$) embryos at both t1 and t5 (*P*-value was not significant, Table S3). (D) Kinesin-1 overexpression attenuates net motion in the plus-end direction. The droplet population shifts inward as additional copies of *halo* are added. (E,F) Average droplet position in the genotypes described in C,D. (G) Staining for Jabba reveals the droplet distribution in 1× *Khc*; 0× *halo*$^{+}$ embryos. The distribution is similar to that observed in *halo* embryos. (H) Average position of droplets in 1× *Khc*; 0× *halo*$^{+}$ and 2× *Khc*; 0× *halo*$^{+}$ embryos. At each time point, the droplet position is indistinguishable (*P*-value was not significant, calculated by performing a *t*-test between the two genotypes at each age class). (E,F,H) Data are presented as mean±s.d. of three embryos. Scale bars: 75 µm (A,B); 7.5 µm (C,D,G). Representative examples of at least three independently performed experiments are shown.

indicating that there was no detectable Halo activity. Yet, when kinesin-1 levels are reduced (1× *Khc* 1× *haloHA*), droplets were more uniformly distributed and did not accumulate near the nuclei (Fig. 7A,B). Quantification reveals a significant inward shift of the droplet population (Table S5), indicating that Halo levels had exceeded the threshold. We conclude that the threshold that allows Halo activity is set by kinesin-1 levels.

Halo and kinesin-1 are present in common complexes

How does the kinesin-1:Halo ratio modulate transport kinetics? There is no evidence that this genetic interaction is due to altered motor copy number or changes in gene expression – kinesin-1 levels are unaffected across phases I, II and III, both in the embryo as a whole and specifically on droplets (Shubeita et al., 2008), and kinesin-1 levels were unchanged in *halo*-mutant embryos (Fig. 7C), indicating that Halo does not alter motor number. Altered kinesin-1 dosage does not alter the expression levels of Halo (Fig. 7E) or overall distribution (Fig. 7D).

When we precipitated Halo from the lysates of Halo–HA-expressing embryos, kinesin was present in the pellets (Fig. 7F). Conversely, Halo–HA was detected in the pellet when kinesin-1 was precipitated (Fig. 7G). Thus, kinesin-1 co-purifies with Halo–HA, suggesting that Halo exists in a complex with kinesin-1. This could be a general property of the Halo protein family as genome-wide interaction studies suggest that other family members can also be complexed with microtubule motors (Guruharsha et al., 2011).

We propose that Halo exerts its effect on kinesin-1 by physically interacting with the motor, directly or indirectly. Thus, Halo might be a limiting kinesin-1 co-factor, and only if it accumulates to fully saturate all droplet motors can transport be fully activated.

DISCUSSION

How bidirectional motion is precisely regulated within the complex cellular environment remains poorly understood. We demonstrate that Halo is the crucial temporal determinant of lipid-droplet transport in *Drosophila* embryos and provide evidence for two levels of temporal control. First, embryos express a transient factor, Halo, the new expression and degradation of which determines the net distribution of droplets. Second, Halo levels temporally and spatially control the position of lipid droplets depending on when Halo surpasses the required threshold to initiate net motion in the plus-end direction. This threshold is set by kinesin-1 levels. Our data suggest a model in which Halo activates kinesin by physically

Journal of Cell Science (2016) 129, 1416-1428 doi:10.1242/jcs.183426

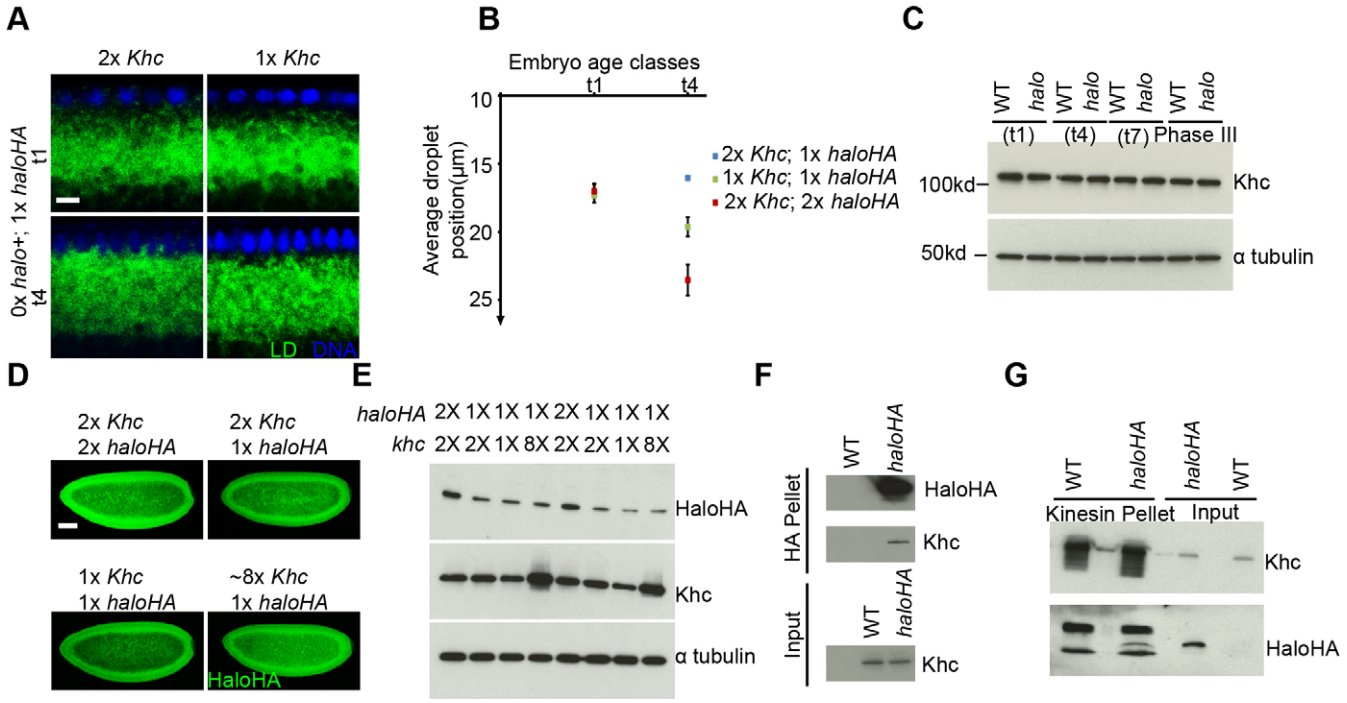

Fig. 7. Kinesin-1 sets the threshold for Halo. (A) Staining for Jabba in 2× *Khc*; 1× *haloHA* (repeated from Fig. 4F for side-by-side comparison) or 1× *Khc*; 1× *haloHA* embryos, with 1× *haloHA* being the only source of Halo function. (B) Average droplet position for the genotypes shown in A. At t1, the average droplet position in both genotypes is similar (*P*-value was not significant, Table S5). At t4, droplets had shifted inward for 1× *Khc* embryos but outward for 2× *Khc* embryos. Data are presented as mean±s.d. of three embryos. (C) Immunoblotting for Khc in embryos at t1, t4, t7 and phase III. Kinesin-1 levels are similar in wild-type (WT) and *halo* embryos. Tubulin serves as loading control. (D,E) HA detection by immunoblotting and immunostaining in embryos expressing 2×, 1× and ∼8× *Khc*. (D) Halo distribution is similar in all genotypes. (E) Blotting for Khc shows the kinesin-1 levels. α-Tubulin is the loading control. Halo levels do not change with Khc dosage. (F) Immunoprecipitation of HA using lysates from wild-type and *haloHA* embryos. Kinesin-1 co-purifies with Halo. (G) Immunoprecipitation of Khc using lysates from wild-type and *haloHA* embryos. Halo co-purifies with kinesin-1. Scale bars: 7.5 µm (A); 75 µm (D). Representative examples of at least three independently performed experiments are shown.

interacting with it, possibly revealing a general regulatory paradigm for bidirectional cargoes.

Quantitative imaging to characterize droplet transport

In *Drosophila* embryos, the intracellular distribution of lipid droplets is highly regulated temporally and spatially. Changes in droplet distribution are typically monitored by altered embryo transparency (Welte, 2015); however, it is challenging to document the dynamic changes at the transitions between phases with this qualitative method. Lipid droplets have also been quantified in sections by using electron microscopy (Welte et al., 1998) or in living embryos by using femtosecond-stimulated Raman loss (fSRL) microscopy (Dou et al., 2012). Although accurate, these methods require specialized equipment and can be quite labour intensive. Here, we combine quantifying the distribution of the lipid-droplet marker Jabba with precise staging of embryos based on morphological criteria. This approach is well suited to document the transitions between phases of transport and can be used to determine the effect not just of Halo but also of other transport regulators.

This quantification provides rich details about the droplet distribution along the apical–basal axis (Fig. 3B,C). Here, we have focused on a single parameter, namely the average position of the droplet population. In the future, analyzing additional features of the distribution, such as its width or skewness, could provide further clues about how the phase transitions are controlled.

Many cell types display precise and temporally modulated positioning of organelles, but rarely are the underlying mechanisms or the significance understood (Van Bergeijk et al., 2016). We show that lipid-droplet position is tightly controlled by Halo levels. Altered droplet distribution in *Drosophila* embryos has so far not been linked to any organismal dysfunction, but it is intriguing that the temporal shifts in droplet transport have been conserved for at least 100 million years (reviewed in Welte, 2015). Droplet movement has been observed in many species and cell types (Welte, 2009). In cultured mammalian cells, regulated redistribution of lipid droplets modulates energy metabolism – upon starvation, droplets disperse along microtubules, leading to increased interactions between droplets and mitochondria, and to efficient transfer of fatty acids between them (Herms et al., 2015). It will be interesting to determine if Halo-driven changes also modulate lipid or protein exchange between droplets and other organelles.

The threshold level for Halo action is set by kinesin-1

The droplet population shifts inward from late phase I through to late phase IIa. We find that this movement is controlled by two different inputs. Redistribution occurs even in the absence of Halo, presumably driven by maternal, as-yet unidentified, factors (Gross et al., 2003). By themselves, these inputs cause net minus-end transport; Halo reverses overall directionality and converts this to net plus-end transport.

During the phase-I to phase-IIa transition, Halo levels rise gradually. Halo affects the droplet-transport machinery only once its levels pass a threshold. With fewer kinesin-1 motors per droplet to turn on, fewer Halo molecules are required to initiate net plus-end transport, suggesting that the threshold is set by the amount of kinesin-1. We propose that once the threshold is crossed, the droplet

Journal of Cell Science (2016) 129, 1416-1428 doi:10.1242/jcs.183426

population moves inward at similar rates, regardless of the levels of Halo and kinesin, and that, depending on when the threshold is crossed, the inward shift occurs with a head start or a delay.

Halo physically interacts with kinesin (Fig. 7F,G) and also activates it in some manner – Halo is required for the phase-IIa-specific increase of droplet travel distances in the plus-end direction (Gross et al., 2003). As Halo levels gradually rise, there should be a period of intermediate Halo levels, sufficient to upregulate some, but not all, of the multiple kinesins present on droplets (Shubeita et al., 2008). However, it is not clear how far droplets will travel that are pulled by both activated (long travel) and unactivated (short travel) motors. Multiple scenarios are conceivable – the most highly processive motor might dominate, promoting long travel; competition between activated and unactivated motors might lead to intermediate travel distances, similar to the compromise in travel characteristics observed for flagellar motors of distinct inherent velocities (Pan et al., 2006); or the short-traveling motors might dominate, if the termination of runs involve a switch (as proposed for droplets; Shubeita et al., 2008; Welte, 2015) that is triggered when the short-traveling motors end their runs. Our results are most consistent with the latter model (Fig. 8B), where droplets with some activated (Halo present) and some unactivated (Halo absent) motors display short travel distances, like droplets with only unactivated motors (Fig. 8A). In this model, long travel distances ensue only once Halo is above the threshold to activate all kinesins (Fig. 8C), and this threshold depends on kinesin, as fewer kinesins per droplet require less Halo for the long-travel state (Fig. 8D). Importantly, once the threshold is surpassed, travel distances are

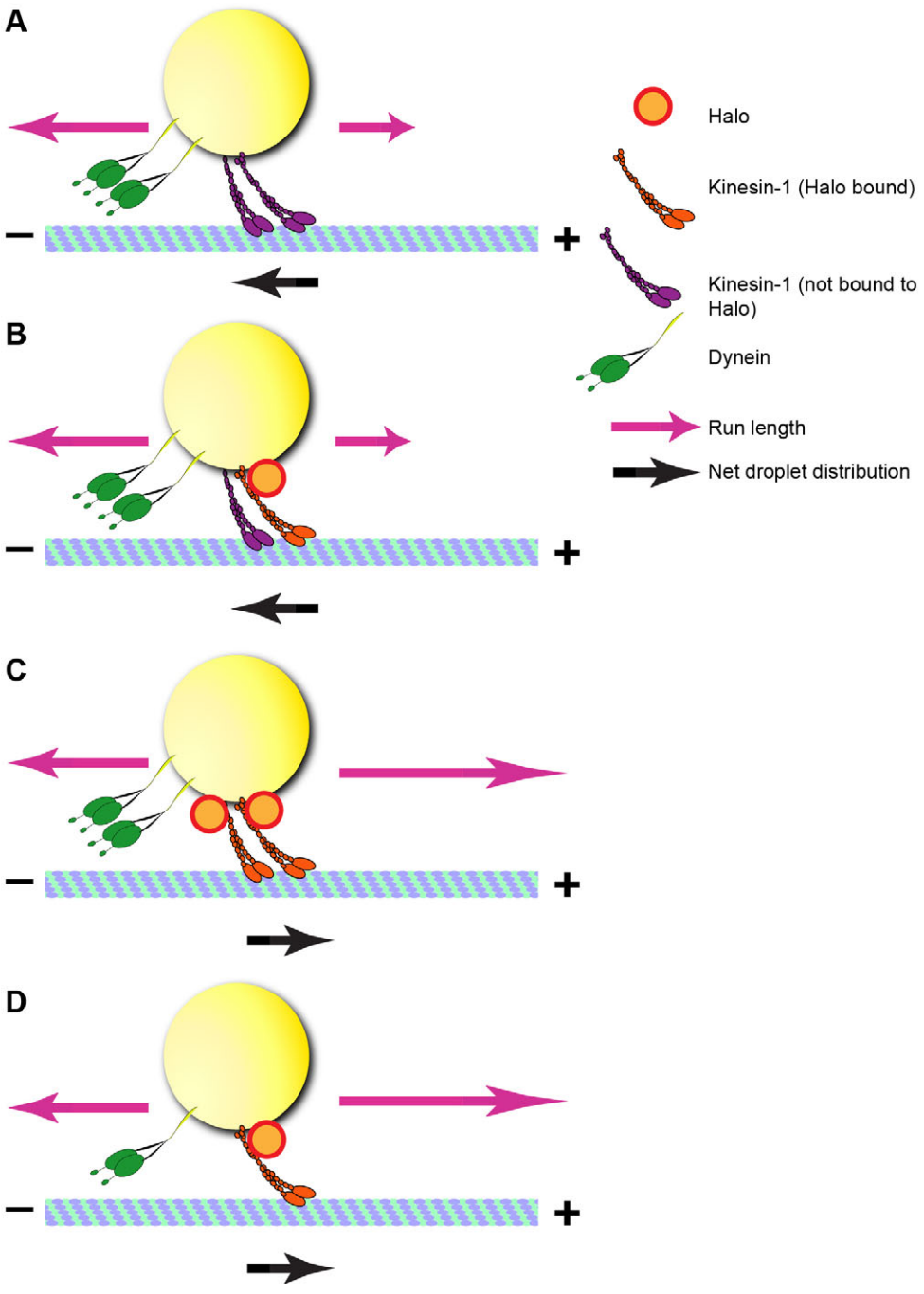

Fig. 8. Model of temporal control of droplet transport. During phase IIa, plus-end run lengths are not upregulated in the absence of Halo (A) or when only a subset of kinesins are activated by Halo binding (B). This lack of upregulation results in net transport in the minus-end direction. (C) Once Halo levels surpass the threshold to bind all kinesins and activate them, plus-end travel distances lengthen, resulting in net plus-end transport. (D) Fewer kinesins per droplet allow full activation at lower Halo levels. A reduction in kinesin-1 levels also reduces the number of active dynein motors (Shubeita et al., 2008). This model does not attempt to incorporate added complexities of how Halo might affect minus-end run lengths (Gross et al., 2003).

Journal of Cell Science (2016) 129, 1416-1428 doi:10.1242/jcs.183426

again independent of motor number, as observed previously (Shubeita et al., 2008).

Much of the Halo protein present is not associated with lipid droplets (Fig. 5B,C). Perhaps Halo is only weakly and transiently bound to droplets and/or motors, dynamically undergoing exchange with a large cytoplasmic pool. Such transient binding might allow rapid reversal of transport at the end of phase IIa, as global reductions of Halo protein levels would result in quick loss of Halo from the motor complexes.

The mechanism of Halo action

Halo does not alter the amount of cargo-bound motors (Shubeita et al., 2008) and, thus, does not act by docking kinesin-1 to or expelling it from droplets. Altered motor–microtubule interactions through modification of tubulin or binding of microtubule-associated proteins are known to affect motor processivity and run lengths (Reed et al., 2006), but currently there is no evidence that the presence of Halo leads to global changes in tracks or their modifications. Halo does not alter the levels of acetylated tubulin, a marker for stable tracks (G.K.A., unpublished observations). Stabilization of the tracks is unlikely to be the mechanism of Halo-mediated upregulation of plus-end run lengths – acetylated tubulin levels increase in phase III (Wolf et al., 1988), even though Halo levels drop and plus-end run lengths are reduced. Halo might therefore act on the proposed 'switching' mechanism that controls engagement and disengagement of motors (Gross et al., 2000; Shubeita et al., 2008; Welte, 2015). Because the switch appears to be sensitive to Halo levels, future dissection of Halo function might provide a molecular inroad into deciphering the mechanism of directional switching.

One clue to the molecular function of Halo is that it is required for the dephosphorylation of LSD-2 during phase IIa (Welte et al., 2005). Because motor behaviour can be altered by phosphorylation (Hirokawa et al., 2009; DeBerg et al., 2013), Halo might control the phosphorylation state of kinesin-1 and, thus, its interaction with the switching mechanism. If Halo is counteracted by a ubiquitous kinase, then it would only be effective if present in high enough concentrations to outperform the kinase, possibly explaining both the threshold effect and the quick reversal of transport once Halo levels drop.

Because the opposing motors on bidirectional cargoes can influence each other both positively and negatively (Hancock, 2014), it is also conceivable that Halo modulates kinesin activity by influencing dynein. Fewer kinesins on droplets results in a parallel decrease of active dynein motors per droplet (Shubeita et al., 2008), and it has been speculated that kinesin and dynein on droplets are present in common complexes (Welte, 2015). Thus, if activation of dynein is the trigger that ends kinesin-1-driven runs (part of the proposed switching mechanism), Halo might extend kinesin-1 run lengths by delaying dynein engagement.

MATERIALS AND METHODS

Fly stocks

The wild-type *Drosophila melanogaster* stock was Oregon R. Among the Drosophila Genetic Reference Panel (DGRP) strains (Mackay et al., 2012), we identified one line, DGRP-392, with a 38-bp deletion in the *halo*-coding region ($halo^{GA}$). $\Delta halo^{AJ}$ has a deletion of ∼19 kb surrounding the *halo* locus, generated using FLP–FRT-mediated recombination (Rembold et al., 2014). Dp(2;2)$halo^{AJ}$ carries two tandem copies of the same region. We varied *halo* dosage levels by using embryos from wild-type mothers crossed to $\Delta halo^{AJ}$ fathers (1× $halo^{+}$), from wild-type parents (2× $halo^{+}$), or from Dp(2;2)$halo^{AJ}$ (4× $halo^{+}$) parents. To analyze *wech*, we employed deletion Df(2R)ST1 (FlyBase ID: FBst0001888), which encompasses the *wech* locus, as well as $wech^{7}$, a missense allele (G at position 544 replaced by S) that we identified using a TILLING approach (Cooper et al., 2008). The *LSD-2*-null allele (FlyBase ID: FBal0131346, Welte et al., 2005) and *Khc*>Khc–GFP (FlyBase ID: FBal0230204, gift from Pernille Rørth, Institute of Molecular and Cell Biology, Singapore; Sung et al., 2008), Khc^{27} (FlyBase ID: FBal0101625, Brendza et al., 1999) and *c-myc-Khc*$^{+}$ (FlyBase ID: FBal0101621, gift of William Saxton, University of California, Santa Cruz, Santa Cruz, CA; de Cuevas et al., 1992; Brendza et al., 1999) flies have been previously described.

Molecular biology

A 3.2-kb genomic region encompassing *halo* [2L:1517488-1520710 (FlyBase release 2015)] was topo-cloned into pCR2.1 (Invitrogen). Using site-directed mutagenesis (Stratagene), a 3×HA tag was inserted after the 92nd amino acid (numbering based on the second AUG). Both the tagged and untagged genomic *halo* constructs were subcloned into pCaSpeR2 (Drosophila Genomics Resource Center). These plasmids were injected into embryos (Genetic Services, Inc.) to generate *p[halo]* and *p[haloHA]* transgenic animals.

Halo-coding regions starting with the first or second AUG (encoded proteins referred to as long Halo and short Halo) were subcloned into pET21a, and a 3×HA tag was introduced. Expression was induced in BL21 cells (Stratagene).

Embryo staging

Embryos were assigned to the four phases – phase I, phase IIa, phase IIb and phase III as previously described (Larsen et al., 2008). We also classified embryos into eight temporal classes. Embryos in age class t0 (phase I) and t1 (phase-I to phase-IIa transition) belong to cycle 12 and cycle13, respectively. t2 to t7 belong to cycle 14. The nuclei are round during t2 and slightly elongated by t3. Classification of t4 to t7 – the membrane has just moved in (t4), is midway down the length of the nuclei (t5), just above (t6) or past (t7) the basal edge of the nuclei. t0 and t1 last for ∼12 and 21 min, respectively (Foe and Alberts, 1983). t2 to t4 represent ∼19 min, followed by ∼6.5 min per age class through t7 (Surkova et al., 2008). For co-immunoprecipitation and lipid-droplet isolation experiments, female flies were allowed to lay eggs for 1 h, and then the embryos were aged for 2.5 h, to enrich the population for phase II.

Immunostaining and microscopy

Embryos were centrifuged to separate lipid droplets from other cellular components (Cermelli et al., 2006; Tran and Welte, 2010). DNA was stained with Hoechst 33258. To immunostain for Jabba, Halo and kinesin-1, embryos were heat-fixed for 1 min and processed using standard procedures (Li et al., 2012). Because heat fixation can selectively extract proteins based on their interactions with other proteins or compartments, it is possible that our centrifugation experiments underestimate the level of Halo in the droplet fraction (Fig. 5B). Anti-Jabba (Li et al., 2012) and anti-Khc (AKIN01-A, Cytoskeleton) antibodies were used at 1:1000. Staining of Jabba is highly specific, as demonstrated by genetic controls (Li et al., 2012). The anti-HA (Clone 3F10; Roche Diagnostics) antibody was used at 1:500 to detect Halo–HA; wild-type embryos served as specificity controls. All secondary antibodies (conjugated with Alexa-Fluor-488 or Alexa-Fluor-594) were obtained from Life Technologies and used at 1:5000. As an alternative way to detect kinesin, wild-type and Khc–GFP-expressing embryos were fixed in 4% formaldehyde for 20 min. Images were acquired on a Leica SP5 confocal microscope using either a 20× or 63× objective. All images were processed in Adobe Photoshop and assembled with Adobe Illustrator.

Quantifying the droplet distribution

Images of Jabba-stained embryos were analyzed with ImageJ – the intensity of the Jabba signal was measured by drawing the region of interest (ROI; straight line tool) from the apical edge of nuclei inwards (about 47 µm deep). For three embryos of the same age class, we measured Jabba intensity along six apically–basally oriented lines, computed – for each line – the normalized intensity as a function of distance, and averaged the six datasets.

This approach estimates what fraction of the droplet population is present at a particular position along the apical–basal axis. For comparison between embryos, we computed the average (mean) distances of the droplet population for a given age class. All data analysis was performed in Microsoft Excel. To compare more than two genotypes, one-way ANOVA, followed by the post-hoc Tukey honest significant difference (HSD) test (pairwise comparisons), was performed. Two genotypes were compared by using Student's unpaired *t*-test. *P*-values ≤0.05 were considered statistically significant. Error bars represent s.d.

In situ hybridization and embryo injection

Embryos were injected with *in-vitro*-generated *halo* mRNA or α-amanitin as described previously (Gross et al., 2003). For *in situ* hybridization, embryos were formaldehyde-fixed and probed as described previously (Wilk et al., 2010). RNA probes were labelled with digoxigenin and detected using NBT/BCIP substrate (Roche). Bright-field images were acquired using the 20× objective on a Nikon Eclipse E600 fluorescence microscope with a 4MP Spot Insight camera.

Western blot analysis and immunoprecipitation

Embryos were heat-fixed, sorted by age and boiled in Laemmli buffer. Proteins were separated using 10% SDS-PAGE gels and transferred to PVDF membranes. Immunodetection was performed using the following primary antibodies – rat anti-HA (1:1000), rabbit anti-Khc (1:1000) and mouse anti-α-Tubulin (T5168, Sigma-Aldrich; 1:10,000) antibodies. All secondary and horseradish peroxidase (HRP)-conjugated antibodies were obtained from Jackson Immuno Research. The specificity of Halo–HA detection was determined by comparison to staining of wild-type embryos. Specificity of Khc detection has been previously demonstrated genetically (Shubeita et al., 2008).

To immunoprecipitate Halo–HA, 250–300 µl of embryos were homogenized in 500 µl 1× PBS, 0.1% Triton, 1 mM DTT, 0.1% NP40 with 1× protease inhibitor cocktail (Sigma-Aldrich). Lysates were cleared (15,500 ***g*** for 30 min), and supernatants were incubated with 10 µl of rat anti-HA or 5 µl anti-Khc antibodies for 12–16 h at 4°C, followed by incubation with 40 µl of a 50% G-protein–Sepharose bead slurry (GE Healthcare) for 4 h. Beads were spun down, washed and subjected to SDS-PAGE and immunodetection.

The lipid-droplet fraction was isolated from whole-embryo lysates according to standard procedures (Li et al., 2012). Equal protein amounts of droplet fraction and lysate were compared by western blotting analysis. LSD-2 was detected using rabbit anti-LSD-2 antibody (at 1:20,000); this antibody was generated previously in our laboratory and specificity of detection was demonstrated genetically (Welte et al., 2005).

Acknowledgements

We thank William Saxton, Pernille Rørth, the Bloomington Stock Center, the Stowers Institute for Medical Research, and the Exelixis stock center at Harvard Medical School for fly stocks, the Developmental Studies Hybridoma Center for antibodies, and the Drosophila TILLING Project for performing the TILLING analysis. We are grateful to Jennifer Einstein for expert technical assistance, to Flavia Sousa for assisting in the cloning of bacterially expressed Halo–HA, and to Danielle Presgraves and James Fry for advice on statistical analysis.

Competing interests

The authors declare no competing or financial interests.

Author contributions

M.A.W., S.L.T. and G.K.A. conceived the project. G.K.A. and S.L.T. designed and performed the bulk of the experiments. G.K.A. performed the imaging and data analysis of the lipid-droplet distribution. N.R. and A.J. generated and characterized some of the mutant fly lines. G.K.A. and M.A.W. prepared the manuscript.

Funding

This work was supported by National Institutes of Health [grant numbers R01GM64687 and R01GM102155 (to M.A.W.)]. Deposited in PMC for release after 12 months.

Supplementary information

Supplementary information available online at http://jcs.biologists.org/lookup/suppl/doi:10.1242/jcs.183426/-/DC1

References

Aspengren, S., Hedberg, D., Sköld, H. N. and Wallin, M. (2009). New insights into melanosome transport in vertebrate pigment cells. *Int. Rev. Cell Mol. Biol.* **272**, 245-302.

Block, S. M. (2007). Kinesin motor mechanics: binding, stepping, tracking, gating, and limping. *Biophys. J.* **92**, 2986-2995.

Bonneaud, N., Savare, J., Berta, P. and Girard, F. (2003). SNCF, a SoxNeuro interacting protein, defines a novel protein family in Drosophila melanogaster. *Gene* **319**, 33-41.

Brendza, K. M., Rose, D. J., Gilbert, S. P. and Saxton, W. M. (1999). Lethal kinesin mutations reveal amino acids important for ATPase activation and structural coupling. *J. Biol. Chem.* **274**, 31506-31514.

Brendza, R. P., Sheehan, K. B., Turner, F. R. and Saxton, W. M. (2000). Clonal tests of conventional kinesin function during cell proliferation and differentiation. *Mol. Biol. Cell* **11**, 1329-1343.

Bullock, S. L., Nicol, A., Gross, S. P. and Zicha, D. (2006). Guidance of bidirectional motor complexes by mRNA cargoes through control of dynein number and activity. *Curr. Biol.* **16**, 1447-1452.

Carter, A. P., Cho, C., Jin, L. and Vale, R. D. (2011). Crystal structure of the dynein motor domain. *Science* **331**, 1159-1165.

Cermelli, S., Guo, Y., Gross, S. P. and Welte, M. A. (2006). The lipid-droplet proteome reveals that droplets are a protein-storage depot. *Curr. Biol.* **16**, 1783-1795.

Cooper, J. L., Till, B. J. and Henikoff,, S. (2008). Fly-TILL: reverse genetics using a living point mutation resource. *Fly (Austin)* **2**, 300-302.

Deberg, H. A., Blehm, B. H., Sheung, J., Thompson, A. R., Bookwalter, C. S., Torabi, S. F., Schroer, T. A., Berger, C. L., Lu, Y., Trybus, K. M. et al. (2013). Motor domain phosphorylation modulates kinesin-1 transport. *J. Biol. Chem.* **288**, 32612-32621.

De Cuevas, M., Tao, T. and Goldstein, L. S. (1992). Evidence that the stalk of Drosophila kinesin heavy chain is an alpha-helical coiled coil. *J. Cell Biol.* **116**, 957-965.

Dou, W., Zhang, D., Jung, Y., Cheng, J.-X. and Umulis, D. M. (2012). Label-free imaging of lipid-droplet intracellular motion in early Drosophila embryos using femtosecond-stimulated Raman loss microscopy. *Biophys. J.* **102**, 1666-1675.

Foe, V. E. and Alberts, B. M. (1983). Studies of nuclear and cytoplasmic behaviour during the five mitotic cycles that precede gastrulation in Drosophila embryogenesis. *J. Cell Sci.* **61**, 31-70.

Gross, S. P., Welte, M. A., Block, S. M. and Wieschaus, E. F. (2000). Dynein-mediated cargo transport in vivo. A switch controls travel distance. *J. Cell Biol.* **148**, 945-956.

Gross, S. P., Welte, M. A., Block, S. M. and Wieschaus, E. F. (2002). Coordination of opposite-polarity microtubule motors. *J. Cell Biol.* **156**, 715-724.

Gross, S. P., Guo, Y., Martinez, J. E. and Welte, M. A. (2003). A determinant for directionality of organelle transport in Drosophila embryos. *Curr. Biol.* **13**, 1660-1668.

Guo, Y., Jangi, S. and Welte, M. A. (2005). Organelle-specific control of intracellular transport: distinctly targeted isoforms of the regulator Klar. *Mol. Biol. Cell* **16**, 1406-1416.

Guruharsha, K. G., Rual, J.-F., Zhai, B., Mintseris, J., Vaidya, P., Vaidya, N., Beekman, C., Wong, C., Rhee, D. Y., Cenaj, O. et al. (2011). A protein complex network of Drosophila melanogaster. *Cell* **147**, 690-703.

Hancock, W. O. (2014). Bidirectional cargo transport: moving beyond tug of war. *Nat. Rev. Mol. Cell Biol.* **15**, 615-628.

Herms, A., Bosch, M., Reddy, B. J. N., Schieber, N. L., Fajardo, A., Rupérez, C., Fernández-Vidal, A., Ferguson, C., Rentero, C., Tebar, F. et al. (2015). AMPK activation promotes lipid droplet dispersion on detyrosinated microtubules to increase mitochondrial fatty acid oxidation. *Nat. Commun.* **6**, 7176.

Hirokawa, N. and Noda, Y. (2008). Intracellular transport and kinesin superfamily proteins, KIFs: structure, function, and dynamics. *Physiol. Rev.* **88**, 1089-1118.

Hirokawa, N., Noda, Y., Tanaka, Y. and Niwa, S. (2009). Kinesin superfamily motor proteins and intracellular transport. *Nat. Rev. Mol. Cell Biol.* **10**, 682-696.

Kon, T., Oyama, T., Shimo-Kon, R., Imamula, K., Shima, T., Sutoh, K. and Kurisu, G. (2012). The 2.8 Å crystal structure of the dynein motor domain. *Nature* **484**, 345-350.

Kull, F. J., Sablin, E. P., Lau, R., Fletterick, R. J. and Vale, R. D. (1996). Crystal structure of the kinesin motor domain reveals a structural similarity to myosin. *Nature* **380**, 550-555.

Larsen, K. S., Xu, J., Cermelli, S., Shu, Z. and Gross, S. P. (2008). BicaudalD actively regulates microtubule motor activity in lipid droplet transport. *PLoS ONE* **3**, e3763.

Lee, K.-D. and Hollenbeck, P. J. (1995). Phosphorylation of kinesin in vivo correlates with organelle association and neurite outgrowth. *J. Biol. Chem.* **270**, 5600-5605.

Li, Z., Thiel, K., Thul, P. J., Beller, M., Kühnlein, R. P. and Welte, M. A. (2012). Lipid droplets control the maternal histone supply of Drosophila embryos. *Curr. Biol.* **22**, 2104-2113.

Loedige, I., Gaidatzis, D., Sack, R., Meister, G. and Filipowicz, W. (2013). The mammalian TRIM-NHL protein TRIM71/LIN-41 is a repressor of mRNA function. *Nucleic Acids Res.* **41**, 518-532.

Mackay, T. F., Richards, S., Stone, E. A., Barbadilla, A., Ayroles, J. F., Zhu, D., Casillas, S., Han, Y., Magwire, M. M., Cridland, J. M., et al. (2012). The Drosophila melanogaster Genetic Reference Panel. *Nature* **482**, 173-178.

Merrill, P. T., Sweeton, D. and Wieschaus, E. (1988). Requirements for autosomal gene activity during precellular stages of Drosophila melanogaster. *Development* **104**, 495-509.

Morfini, G., Szebenyi, G., Brown, H., Pant, H. C., Pigino, G., DeBoer, S., Beffert, U. and Brady, S. T. (2004). A novel CDK5-dependent pathway for regulating GSK3 activity and kinesin-driven motility in neurons. *EMBO J.* **23**, 2235-2245.

Pan, X., Ou, G., Civelekoglu-Scholey, G., Blacque, O. E., Endres, N. F., Tao, L., Mogilner, A., Leroux, M. R., Vale, R. D. and Scholey, J. M. (2006). Mechanism of transport of IFT particles in C. elegans cilia by the concerted action of kinesin-II and OSM-3 motors. *J. Cell Biol.* **174**, 1035-1045.

Pilot, F., Philippe, J.-M., Lemmers, C., Chauvin, J.-P. and Lecuit, T. (2006). Developmental control of nuclear morphogenesis and anchoring by charleston, identified in a functional genomic screen of Drosophila cellularisation. *Development* **133**, 711-723.

Reck-Peterson, S. L., Yildiz, A., Carter, A. P., Gennerich, A., Zhang, N. and Vale, R. D. (2006). Single-molecule analysis of dynein processivity and stepping behavior. *Cell* **126**, 335-348.

Reed, N. A., Cai, D., Blasius, T. L., Jih, G. T., Meyhofer, E., Gaertig, J. and Verhey, K. J. (2006). Microtubule acetylation promotes kinesin-1 binding and transport. *Curr. Biol.* **16**, 2166-2172.

Rembold, M., Ciglar, L., Yanez-Cuna, J. O., Zinzen, R. P., Girardot, C., Jain, A., Welte, M. A., Stark, A., Leptin, M. and Furlong, E. E. M. (2014). A conserved role for Snail as a potentiator of active transcription. *Genes Dev.* **28**, 167-181.

Sheng, Z.-H. (2014). Mitochondrial trafficking and anchoring in neurons: new insight and implications. *J. Cell Biol.* **204**, 1087-1098.

Shubeita, G. T., Tran, S. L., Xu, J., Vershinin, M., Cermelli, S., Cotton, S. L., Welte, M. A. and Gross, S. P. (2008). Consequences of motor copy number on the intracellular transport of kinesin-1-driven lipid droplets. *Cell* **135**, 1098-1107.

Sung, H. H., Telley, I. A., Papadaki, P., Ephrussi, A., Surrey, T. and Rorth, P. (2008). Drosophila ensconsin promotes productive recruitment of Kinesin-1 to microtubules. *Dev. Cell* **15**, 866-876.

Surkova, S., Myasnikova, E., Janssens, H., Kozlov, K. N., Samsonova, A. A., Reinitz, J. and Samsonova, M. (2008). Pipeline for acquisition of quantitative data on segmentation gene expression from confocal images. *Fly* **2**, 58-66.

Tran, S. L. and Welte, M. A. (2010). *In-vivo* centrifugation of Drosophila embryos. *J. Vis. Exp.*, **40**, e2005.

Vale, R. D. (2003). The molecular motor toolbox for intracellular transport. *Cell* **112**, 467-480.

Van Bergeijk, P., Hoogenraad, C. C. and Kapitein, L. C. (2016). Right time, right place: probing the functions of organelle positioning. *Trends Cell Biol.* **26**, 121-134. Epub 2015 Nov 2.

Welte, M. A. (2004). Bidirectional transport along microtubules. *Curr. Biol.* **14**, R525-R537.

Welte, M. A. (2009). Fat on the move: intracellular motion of lipid droplets. *Biochem. Soc. Trans.* **37**, 991-996.

Welte, M. A. (2015). As the fat flies: the dynamic lipid droplets of Drosophila embryos. *Biochim. Biophys. Acta* **1851**, 1156-1185.

Welte, M. A., Gross, S. P., Postner, M., Block, S. M. and Wieschaus, E. F. (1998). Developmental regulation of vesicle transport in Drosophila embryos: forces and kinetics. *Cell* **92**, 547-557.

Welte, M. A., Cermelli, S., Griner, J., Viera, A., Guo, Y., Kim, D.-H., Gindhart, J. G. and Gross, S. P. (2005). Regulation of lipid-droplet transport by the perilipin homolog LSD2. *Curr. Biol.* **15**, 1266-1275.

Wilk, R., Murthy, S. U. M., Yan, H. and Krause, H. M. (2010). In situ hybridization: fruit fly embryos and tissues. *Curr. Protoc. Essent. Lab. Tech.* 4, 9.3.1-9.3.24.

Wolf, N., Regan, C. L. and Fuller, M. T. (1988). Temporal and spatial pattern of differences in microtubule behaviour during Drosophila embryogenesis revealed by distribution of a tubulin isoform. *Development* **102**, 311-324.

Yildiz, A., Tomishige, M., Gennerich, A. and Vale, R. D. (2008). Intramolecular strain coordinates kinesin stepping behavior along microtubules. *Cell* **134**, 1030-1041.